http://dx.doi.org/10.5012/bkcs.2014.35.3.775

Spin-orbit Effects on the Structure of Haloiodomethane Cations CH_2XI^+ (X=F, Cl, Br, and I)†

Hyoseok Kim, Young Choon Park, and Yoon Sup Lee*

*Department of Chemistry KAIST, Daejeon 305-701, Korea. *E-mail: yslee@kaist.edu*
Received August 23, 2013, Accepted September 9, 2013

The importance of including spin-orbit interactions for the correct description of structures and vibrational frequencies of haloiodomethanes is demonstrated by density functional theory calculations with spin-orbit relativistic effective core potentials (SO-DFT). The vibrational frequencies and the molecular geometries obtained by SO-DFT calculations do not match with the experimental results as well as for other cations without significant relativistic effects. In this sense, the present data can be considered as a guideline in the development of the relativistic quantum chemical methods. The influence of spin-orbit effects on the bending frequency of the cation could well be recognized by comparing the experimental and calculated results for CH_2BrI and CH_2ClI cations. Spin-orbit effects on the geometries and vibrational frequencies of CH_2XI (X=F, Cl, Br, and I) neutral are negligible except that C-I bond lengths of haloiodomethane neutral is slightly increased by the inclusion of spin-orbit effects. The $^2A'$ and $^2A''$ states were found in the cations of haloiodomethanes and mix due to the spin-orbit interactions and generate two $^2E_{1/2}$ fine-structure states. The geometries of CH_2XI^+ (X=F and Cl) from SO-DFT calculations are roughly in the middle of two cation geometries from DFT calculations since two cation states of CH_2XI (X=F and Cl) from DFT calculations are energetically close enough to mix two cation states. The geometries of CH_2XI^+ (X=Br and I) from SO-DFT calculations are close to that of the most stable cation from DFT calculations since two cation states of CH_2XI (X=Br and I) from DFT calculations are energetically well separated near the fine-structure state minimum.

Key Words : Haloiodomethane, Haloiodomethane cation, Spin-orbit effect, Density functional theory

Introduction

Quantum chemical calculations could provide results comparable to experimental measurements in many instances, but still need improvement in the accuracy and reliability. One such direction is the inclusion of spin-orbit interactions in Hamiltonian. The importance of relativity for the description of heavy elements is well recognized,[1-3] and the spin-orbit interaction is present in the relativistic formalism based upon Dirac operator for the electron. Spin-orbit and other relativistic effects required for the accurate description of valence states of molecules containing heavy elements can be represented as two-component relativistic effective core potentials (RECPs) derived from Dirac-Coulomb Hamiltonian based all-electron calculations of atoms.[4] Scalar relativistic effects are routinely included in electronic-structure calculations through the use of RECPs, but spin–orbit interactions are usually omitted when deriving optimized structures partly because of the assumption that their influence on the molecular structures is negligible and partly due to computational difficulties.[5,6] Even when spin–orbit terms are available in RECPs, the usual treatment involves perturbational inclusion of these terms after the variational determination of orbitals and structures. Quantum chemical calculations employing RECPs with spin–orbit operators from the beginning of *ab initio* calculations have been available.[7,8] Spin–orbit density functional theory (SO-DFT) method available in NWCHEM is particularly useful for the present purpose of demonstrating spin–orbit effects on geometries since the structures can be optimized with both spin–orbit interactions and electron correlations included.[9,10] Relativistic effects on geometries of molecules containing heavy elements can be comparable or larger than electron correlation effects and make an unexpected shape to be a local minimum. We found this influence of spin-orbit interactions on the geometry for polyhalomethanes CH_2ClI^+ and $CH2BrI^+$ cations in collaborations with the group of Prof. M. S. Kim.[11-13]

Polyhalomethanes have been of considerable interest in relation to ozone depletion in the atmosphere.[14-16] The photochemistry of iodine containing polyhalomethanes such as CH_2ClI, CH_2BrI, and CH_2I_2 have been actively investigated in this context for the role in the ozone depletion in the troposphere,[15,17,18] and also from the point of view of fundamental science for the importance of these molecules as prototypes of the reaction control *via* electronic state selection.[19-21] Another important aspect in the fundamental study of these iodine containing molecules is the extent of the influence of relativistic effects on their structures and molecular properties.[11,12] A conventional approach to handle this effect in the electronic structure calculation is to adopt RECPs for heavy elements. Spin-orbit interaction is usually omitted as noted above. The same approach is generally adopted to analyze the results from the photoelectron spectro-

†This paper is to commemorate Professor Myung Soo Kim's honourable retirement.

scopy (PES) which provides low resolution spectroscopic data for cations.[22,23] Zero kinetic energy (ZEKE) photoelectron spectroscopy[24,25] and mass-analyzed threshold ionization (MATI) spectroscopy[26] are offspring of PES and provide much higher resolution spectroscopic data for cations. The vibrational spectra of the halomethane cations have been recorded using the MATI spectrometry.[11-13] SO-DFT calculations for spectroscopic constants of mixed dihalomethanes have been performed using shape-consistent RECPs with effective one-electron spin-orbit operator to confirm and improve the phenomenological assignments.

In order to generalize and understand interesting spin-orbit effects obtained for CH_2ClI^+ and CH_2BrI^+, we extend the study to include CH_2FI^+ and $CH_2I_2^+$. The vibrational frequencies of CH_2XI (X=F, Cl, Br, and I) neutral and cation were obtained from SO-DFT calculations. The shapes and energy levels of molecular orbitals from DFT calculations and the energy levels of molecular spinors from SO-DFT calculations were analyzed to reveal the origin of characteristic spin-orbit effects on the X-C-I bond angle.

Computational Details

Optimized molecular geometries of haloiodomethane CH2XI neutral and cation (X=F, Cl, Br, and I) were calculated at the DFT level of theory employing RECPs including spin-orbit terms. The RECP employed for the present calculations is expressed by the following form within the framework originated from Lee *et al*.,[27]

$$U^{REP} = U_{LJ}^{REP}(r) + \sum_{l=0}^{L-1} \sum_{j=\left|l-\frac{1}{2}\right|}^{l+\frac{1}{2}} \sum_{m=-j}^{j} [U_{lj}^{REP}(r) - U_{LJ}^{REP}(r)] |ljm\rangle\langle ljm| \quad (1)$$

where $|ljm\rangle\langle ljm|$ represents a two-component projection operator. Molecular spinors which are obtained as one-electron wave functions of the Hamiltonian containing the above RECP have two components. The RECP, U^{REP} which is referred to SOREP here can be expressed as the sum of the scalar relativistic effective core potential (AREP), U^{AREP}, and the effective one-electron spin-orbit operator,[28] U^{SO}, as

$$U^{REP} = U^{AREP} + U^{SO} \quad (2)$$

Values calculated with AREP include scalar relativistic effects, and those with SOREP contain spin-orbit effects as well as scalar relativistic effects. The spin-orbit effects (Δ_{SO}) are defined as the difference between AREP and SOREP values calculated with the same basis set at a given level of theory.

SO-DFT calculations were done for the CH_2XI (X=F, Cl, Br, and I) neutral and cation in the ground electronic state with the B3LYP[29] (Becke's three parameter hybrid functional[30] with the Lee-Yang-Parr correlation functional[31]) functional using NWCHEM.[9,10] RECPs with the effective spin-orbit potentials and the basis sets for the valence shell reported by Christiansen and coworkers[32,33] were used for halogen atoms. To this basis set of F, Cl, Br, and I, the diffuse and polarization functions reported by Lee *et al*.[5] were added to make halogen basis sets consistent with the large basis sets used for other atoms as shown in Table 1. AREP and SOREP calculations were performed to observe the magnitude of spin-orbit effects. The step size in the calculation of the numerical Hessian was optimized to produce reliable vibrational frequencies. Equilibrium geometries and vibrational frequencies of the neutral and the cation were calculated.

Table 1. Basis sets and RECPs used in the SO-DFT calculations with the B3LYP functional[a]

set	RECP	basis set	
	halogen atom (X)	halogen atom (X)	other atoms
1	7 VE CRENBL RECP for F	*4s4p3d2f* basis set for F	aug-cc-pVTZ
	7 VE CRENBL RECP for Cl	*4s4p3d2f* basis set for Cl	
	17 VE CRENBL RECP for Br	*4s4p6d2f* basis set for Br	
	17 VE CRENBL RECP for I	*4s4p6d2f* basis set for I	

[a]RECPs and basis sets used for halogen atoms are in Refs. 32 and 33 and spin-orbit terms in the same references were used when needed.

Six sets of DFT calculations were performed for CH_2ClI to test the effects of the type of functionals. The applied hybrid functionals were B3LYP,[29] ACM[30] (Becke's adiabatic connection method, also known as B3PW91) and PBE0[34,35] (Perdew-Burke-Ernzerhof parameter-free functional) functionals. Additional DFT calculations use local density approximation (LDA), generalized gradient approximation (GGA), and hybrid meta-GGA (HMGGA) of the exchange-correlation functionals to gauge the reliability of the hybrid functionals. The applied LDA and GGA functionals are SVWN5 (Slater exchange[36] and Vosko-Wilk-Nusair correlation functional (VWN)[37]), BP86 (Becke exchange[38] and Perdew correlation functional[39]), respectively. The applied HMGGA functionals is M05[40] (Minnesota 2005). It is noted that RECPs used here are all generated using relativistic HF results and may introduce some inconsistency when used with DFT methods. We assume this error to be small enough at least for the purposes of the present study.

Results and Discussion

Test Calculations for CH_2ClI. DFT calculations with several functionals were performed for CH_2ClI and optimized geometrical parameters are listed in Table 2. There are the functional dependencies on the bond lengths of CH_2ClI neutral, while that on the bond angles are small as shown in Table 2. Spin-orbit effects on the geometries of CH_2ClI neutral are negligible except on the C-I bond lengths for which spin-orbit effects slightly increase the bond length. The most pronounced discrepancy from experimental geometrical parameters is the C-I bond length. All calculated C-I bond

Table 2. Geometries of CH_2ClI neutral in the ground electronic state without (w/o) and with (w/) spin-orbit effects[a]

Method		bond length (Å)			bond angle (°)			
		C–Cl	C–I	C–H	Cl–C–I	Cl–C–H	I–C–H	H–C–H
exp.[b]		1.774	2.137	1.062	112.5	108.4	108.3	111.0
HF	w/o	1.760	2.139	1.072	113.9	108.8	106.8	111.9
	w/	1.760	2.142	1.072	113.9	108.8	106.7	111.9
SVWN5	w/o	1.758	2.154	1.095	114.2	109.1	106.3	111.7
	w/	1.757	2.159	1.095	113.9	109.2	106.5	111.6
BP86	w/o	1.782	2.191	1.091	114.4	108.7	106.5	112.1
	w/	1.781	2.197	1.091	114.4	108.8	106.3	112.2
B3LYP	w/o	1.778	2.181	1.081	114.4	108.6	106.6	112.1
	w/	1.777	2.187	1.081	114.4	108.7	106.6	112.0
ACM	w/o	1.766	2.163	1.083	114.3	108.8	106.6	111.8
	w/	1.765	2.168	1.083	114.3	108.9	106.5	111.8
PBE0	w/o	1.759	2.154	1.084	114.2	108.9	106.6	111.7
	w/	1.760	2.157	1.084	114.0	108.9	106.7	111.6
M05	w/o	1.765	2.152	1.083	114.7	108.6	106.9	111.2
	w/	1.765	2.156	1.083	114.7	108.6	106.9	111.3

[a]The set **1** basis sets and RECPs in Table 1 were used. [b]Microwave spectroscopic data from Ref.[42]

Table 3. Geometries of CH_2ClI cation in the ground electronic state without (w/o) and with (w/) spin-orbit effects[a]

Method		bond length (Å)			bond angle (°)			
		C–Cl	C–I	C–H	Cl–C–I	Cl–C–H	I–C–H	H–C–H
HF	$^2A'$	1.713	2.267	1.073	106.8	113.5	102.8	115.7
	$^2A''$	1.701	2.283	1.075	112.4	114.0	100.1	114.4
	$^2E_{1/2}$	1.707	2.278	1.073	110.0	113.8	101.3	115.0
SVWN5	$^2A'$	1.761	2.144	1.096	93.1	111.9	110.1	115.7
	$^2A''$	1.711	2.141	1.111	119.5	111.1	103.8	106.5
	$^2E_{1/2}$	1.751	2.156	1.097	97.5	112.2	109.4	114.8
BP86	$^2A'$	1.779	2.188	1.092	94.9	111.7	110.2	116.1
	$^2A''$	1.726	2.198	1.104	118.7	111.4	102.6	109.2
	$^2E_{1/2}$	1.765	2.207	1.093	99.8	112.1	108.2	115.3
B3LYP	$^2A'$	1.767	2.187	1.082	96.1	111.9	109.7	115.8
	$^2A''$	1.715	2.245	1.090	116.1	113.1	101.0	111.6
	$^2E_{1/2}$	1.738	2.242	1.084	106.0	112.7	104.9	114.5
ACM	$^2A'$	1.760	2.161	1.084	94.8	112.0	110.2	115.7
	$^2A''$	1.710	2.205	1.093	116.3	112.9	101.5	110.7
	$^2E_{1/2}$	1.744	2.187	1.085	101.0	112.4	107.6	114.7
PBE0	$^2A'$	1.755	2.151	1.085	94.5	112.0	110.3	115.7
	$^2A''$	1.707	2.194	1.093	115.8	113.0	101.6	110.7
	$^2E_{1/2}$	1.741	2.174	1.086	100.1	112.4	108.0	114.7
M05	$^2A'$	1.760	2.144	1.083	94.1	111.8	110.9	115.4
	$^2A''$	1.714	2.164	1.093	117.2	112.2	102.5	109.2
	$^2E_{1/2}$	1.748	2.163	1.084	99.3	112.1	108.8	114.6

[a]The set **1** basis sets and RECPs in Table 1 were used.

lengths of CH_2ClI from DFT and SO-DFT calculations are overestimated compared to the experimental ones. The C-I bond lengths of CH_2ClI from HF and SO-HF calculations are closer to the experimental one. The C-I bond lengths of CH_2ClI from DFT calculations have rather small variation with the class of the functional employed among LDA, GGA and HGGA. LDA yields shortest one followed by HGGA and then GGA. Roughly speaking, the C-I bond lengths of CH_2ClI from DFT calculations with functionals including HF exchange contribution, which are hybrid functionals, are indirectly proportional to the amount of the HF exchange contribution to the functionals. The C-I bond lengths of CH_2ClI from DFT calculations with functionals including HF exchange contribution are 2.181 (B3LYP with 20% HF exchange), 2.163 (ACM or B3PW91 with 20% HF exchange), 2.154 (PBE0 with 25% HF exchange), 2.152

(M05 with 28% HF exchange), and 2.151 (BHLYP with 50% HF exchange). The hybrid functional with the larger HF exchange results in the shorter C-I bond length and closer to experimental one. The vibrational frequencies of CH_2ClI neutral from DFT calculations with hybrid functional are overestimated compared to experimental ones. Since HF results for energies and vibrational frequencies are not reliable, we may select DFT and hybrid functionals among DFT as the method of choice for chloroiodomethane.

Two stationary states, ^{2}A' and ^{2}A", of the chloroiodomethane cation corresponding to removal of HOMO$_{-1}$ a' and HOMO a'', respectively, from the neutral molecule can be obtained in AREP-HF and AREP-DFT calculations. The optimized structures of the two cation states indicate that structural change from the neural one is larger for the ^{2}A' state than for the ^{2}A" state, It appears that antibonding interaction for the a' orbital is larger than that in the a'' orbital as can be seen in Figure 1. Reflecting this larger geometry changes, the most stable cation of CH_2ClI is the ^{2}A' state generated by removal of an electron from the second highest occupied a' orbital (Fig. 1). Qualtitative changes from neutral to the two cation states in Table 3 are essentially similar for all methods. One exception is the C-I bond length. HF gives longer bond lengths for cation states while LDA and GGA produce shorter ones for the cation states. It appears that electron correlations shorten the C-I bond lengths, which is also observed in all-electron calculations.[41] It is noted that this trend is opposite to that in the neutral. The ^{2}A' and ^{2}A" states mix due to the spin-orbit interactions and generate two $^2E_{1/2}$ fine-structure states. The energy differences of two cation states from AREP calculations for CH_2ClI^+ is about 1200 cm^{-1}. Energetically close two states of chloroiodomethane cation mix substantially to generate the fine-structure states with geometries somewhere between two AREP states. The geometries of CH_2ClI from SO-DFT calculations are roughly in the middle of two cation geometries especially in terms of the Cl-C-I bond angle. In this regard, HF and all DFT functional considered afford the same trend. This has been the subject of several reports. We try to observe the general pattern of this behavior by considering other members of CH_2XI^+, The performance of HF and various DFT methods for the cation is similar to that for the neutral case and we proceed to use B3LYP with AREP and SOREP for other members of CH_2XI.

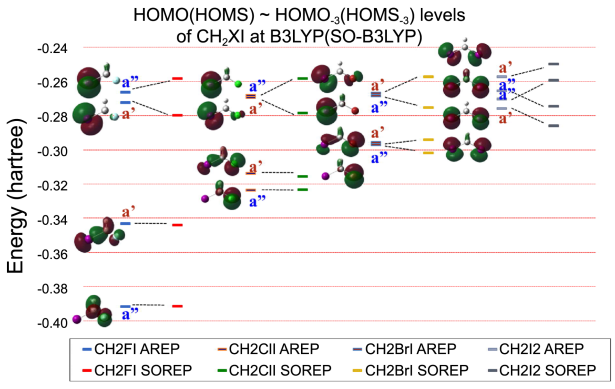

Figure 1. Shapes and energy levels (energy levels) of molecular orbitals (molecular spinors) from the B3LYP (SO-B3LYP) calculations for CH_2XI (X=F, Cl, Br, and I). For each molecule orbital energy levels are on the left column and molecular spinor energy levels are open the right. Each dotted line connecting an orbital with a spinor imply spin-orbit coupling.

Spin-orbit Effects on the Vibrational Frequencies of Haloiodomethane Cations (CH_2XI^+ (X=F, Cl, Br, and I)). Spin-orbit effects on the geometries and vibrational frequencies of CH_2XI (X=F, Cl, Br, and I) neutral are negligible as shown in Tables 4 and 5. The C-I bond length of haloiodomethane neutral is slightly increased by the inclusion of spin-orbit effects. Calculations incorporating spin-orbit terms still need to achieve more accurate theoretical results. The calculated C-I bond lengths of CH_2ClI and CH_2I_2 are overestimated in comparison to the available experimental ones.[42,43] The calculated C-I bond lengths of CH_2BrI and CH_2I_2 are longer than the available CASPT2 results.[44,45] DFT calculations with the B3LYP functional using RECPs by Christiansen *et al*.[32,33] seem to overestimate the C-I bond lengths, but the degree of overestimate is not so large as to affect the reliability of the present study. The C-X bond lengths of CH_2XI (X=F, Cl, Br, and I) increase on descending the halogen group in the periodic table, as expected from the increasing size of halogen atoms. The C-I bond lengths of CH_2XI (X=F, Cl, Br, and I) decrease on descending the halogen group in the periodic table. The X-C-I bond angle of CH_2XI (X=F, Cl, Br, and I) increases on descending the halogen group in the periodic table probably due to the increasing steric repulsion between X and I. In order to reduce the steric repulsion between X and I, the shorter C-X bond length induces the longer C-I bond length. The X-C-I bond angle of CH_2I_2 is also larger than that of CH_2FI indicating that the steric repulsion between Two I atoms is larger than that between F and I atoms.

The shapes and energy levels of molecular orbitals and energy levels of molecular spinors of CH_2XI (X=F, Cl, Br, and I) neutral are shown in Figure 1. For CH_2XI (X=F and Cl), HOMO and HOMO$_{-1}$ have a'' and a' symmetries, respectively. For CH_2BrI and CH_2I_2, HOMO and HOMO$_{-1}$ have a' and a'' symmetries, respectively. The a' and a'' correspond largely to the iodine 5p nonbonding orbtials, parallel n(I5$p_{\|}$) and perpendicular n(I5$p_{\perp}$), respectively, to the molecular plane as shown in Figure 1. The a' orbitals are two in-plane nonbonding orbitals, n(I5$p_{\|}$) and n(X$np_{\|}$). The in-plane nonbonding orbitals of two halogens have small antibonding interactions with each other The antibonding characteristics of a' orbitals for CH_2XI (X=F, Cl, Br, and I) increase on descending the periodic table. Thus the energy levels of molecular orbitals increase for the lower members of the halogen group in the periodic table. The a'' orbitals have the perpendicular nonbonding orbital, n(I5$p_{\perp}$). The energy levels of molecular orbitals are all similar in CH_2XI (X=F, Cl, Br, and I). As a result, the destabilization of a' orbitals induces the symmetry alternation of HOMO and HOMO$_{-1}$ in CH_2XI (X=Br and I) compared with CH_2XI (X=F and Cl). Thus the gap in energy levels of HOMO and HOMO$_{-1}$ in CH_2ClI

Table 4. Geometries of CH_2XI (X = F, Cl, Br, and I) neutral in the ground electronic state calculated without (w/o) and with (w/) spin-orbit interactions[a]

		bond length (Å)			bond angle (°)			
		C–X	C–I	C–H	X–C–I	X–C–H	I–C–H	H–C–H
CH_2FI	w/o	1.368	2.188	1.085	111.1	109.7	106.8	112.9
	w/	1.368	2.193	1.085	111.0	109.6	106.7	113.1
CH_2ClI	w/o	1.778	2.181	1.081	114.4	108.6	106.6	112.1
	w/	1.777	2.187	1.081	114.4	108.7	106.6	112.0
	exp.[b]	1.774	2.137	1.062	112.5	108.4	108.3	111.0
CH_2BrI	w/o	1.953	2.172	1.080	115.1	107.6	107.3	112.1
	w/	1.954	2.176	1.080	115.0	107.7	107.2	112.2
	calc.[c]	1.946	2.155	1.094	115.3	107.4	107.5	111.8
	calc.[d]	1.956	2.172	1.098	114.3			111.4
	calc.[e]	1.935	2.130	1.091	113.2			112.3
CH_2I_2	w/o	2.170	2.170	1.081	116.4	107.2	107.2	111.7
	w/	2.175	2.175	1.081	116.3	107.3	107.3	111.7
	calc.[f]	2.174	2.174	1.086	116.4	107.0	107.0	112.5
	calc.[g]	2.158	2.158	1.086	115.2			111.8
	calc.[h]	2.143	2.143	1.086	115.9	107.5	107.5	111.2
	calc.[i]	2.135	2.135	1.093	114.7	107.6	107.6	111.7
	exp.[j]	2.12	2.12	1.09	114.7			111.3

[a]The set **1** basis sets and RECPs in Table 1 were used. [b]Microwave spectroscopic data from Ref.[42] [c]B3LYP/Sadlej-PVTZ calculations from Ref.[46] [d]CASSCF/ANO-RCC calculations from Ref.[44] [e]CASPT2/ANO-RCC calculations from Ref.[44] [f]BLYP calculations from Ref.[47] [g]MP2 calculations from Ref.[48] [h]QCISD calculations from Ref.[49] [i]CASPT2L1 calculations from Ref.[45] [j]Ref.[43]

Table 5. Vibrational frequencies (in cm^{-1}) of CH_2XI (X = F, Cl, Br, and I) neutral in the ground electronic state calculated without (w/o) and with (w/) spin-orbit interactions[a]

		a′						*a″*		
		ν_1[b]	ν_2	ν_3	ν_4	ν_5	ν_6	ν_7	ν_8	ν_9
CH_2FI	w/o	3094	1483	1284	1050	553	259	3175	1238	847
	w/	3093	1482	1282	1049	547	257	3176	1238	843
CH_2ClI	w/o	3126	1439	1202	707	523	188	3207	1128	782
	w/	3126	1439	1202	709	518	186	3207	1127	780
	exp.[c]	2978	1392	11l83	718	527	194	3048	1126	801
	exp.[d]	3001	1412	1188	740	536	192	3066	1108	789
CH_2BrI	w/o	3138	1426	1173	605	511	138	3213	1085	764
	w/	3133	1421	1172	604	507	137	3218	1079	755
	calc.[e]	3108	1393	1154	612	522	143	3203	1077	746
	calc.[f]	3050	1471	1194	622	517	140	3137	1100	795
	calc.[g]	3122	1424	1221	647	550	143	3182	1075	787
	exp.[h]	2978	1374	1150	616	517	144	3053	1065	754
CH_2I_2	w/o	3137	1407	1123	563	474	113	3212	1043	713
	w/	3130	1408	1117	555	469	111	3214	1037	700
	exp.[c]	2983	1361	1152	580	492	122	3063	1033	714
	exp.[i]	2968	1369		581	493	134	3049	1028	714

[a]The set **1** basis sets and RECPs in Table 1 were used. [b]Mulliken notation. [c]Raman spectroscopic data from Ref.[50] [d]Raman spectroscopic data from Ref.[51] [e]B3LYP/Sadlej-PVTZ data from Ref.[46] [f]CASSCF/ANO-RCC calculations from Ref.[44] [g]CASPT2/ANO-RCC calculations from Ref.[44] [h]Raman spectroscopic data from Ref.[19] [i]Raman spectroscopic data from Ref.[52]

(299 cm^{-1}) and CH_2BrI (379 cm^{-1}) are closer than that in CH_2FI (1302 cm^{-1}) and CH_2I_2 (1813 cm^{-1}). The HOMO and $HOMO_{-1}$ levels in DFT calculations shift due to spin-orbit interactions and generate highest occupied molecular spinor (HOMS) and $HOMS_{-1}$ in SO-DFT calculations. Actually all energy levels are affected by spin-orbit interactions. The closer the energy levels in DFT calculations, the larger the spin-orbit splitting in SO-DFT calculations. The splitting of HOMS and $HOMS_{-1}$ energy levels due to spin-orbit effects are 4751 cm^{-1} for CH_2FI, 4448 cm^{-1} for CH_2ClI, 3956 cm^{-1} for CH_2BrI, and 5402 cm^{-1} for CH_2I_2.

Similar analysis is possible for lower lying halogen orbitals.

For CH_2XI (X=F, Cl, and Br), $HOMO_{-2}$ and $HOMO_{-3}$ have a' and a'' symmetries, respectively. For CH_2I_2, $HOMO_{-2}$ and $HOMO_{-3}$ have a'' and a' symmetries, respectively. The a' and a'' orbitals correspond to the antibonding combination of mainly nobonding orbitals parallel and perpendicular to the molecular plane, respectively, as shown in Figure 1. The a' orbitals have two in-plane orbitals a($I5p_{\|}$) and a($Xnp_{\|}$) in antibonding combination. The antibonding characters of a' orbitals for CH_2XI (X=F, Cl, Br, and I) increase on descending the halogen group in the periodic table in line with increase in the energy levels of molecular orbitals. The a'' orbitals comprise the perpendicular nonbonding orbital, n($I5p_{\perp}$), n($Xnp_{\|}$) and small contributions from the CH_2 fragment. The perpendicular nonbonding orbitals of two halogens have slight antibonding interactions with each other. The antibonding characters of a'' orbitals for CH_2XI (X=F, Cl, Br, and I) also increase on descending the halogen group in the periodic table, and the energy levels of molecular orbitals rise on descending the halogen group in the periodic table. The extent of the destabilization of a'' orbitals is faster than that of a' orbitals, which results in the symmetry alternation of $HOMO_{-2}$ and $HOMO_{-3}$ in CH_2I_2 in comparison to CH_2XI (X=F, Cl, and Br). The destabilization of $HOMO_{-2}$ and $HOMO_{-3}$ is faster than that of HOMO and $HOMO_{-1}$. For CH_2I_2, the energy levels of HOMO, $HOMO_{-1}$, $HOMO_{-2}$, and $HOMO_{-3}$ are quite close.

The spin-orbit splitting of the $HOMO_{-2}$ and $HOMO_{-3}$ levels to the $HOMS_{-2}$ and $HOMS_{-3}$ levels strongly depends on the X halogen atom. The energy levels of $HOMO_{-2}$ and $HOMO_{-3}$ for CH_2XI (X=F and Cl) are similar to those of $HOMS_{-2}$ and $HOMS_{-3}$, reflecting small spin-orbit splittings of F and Cl. The $HOMO_{-2}$ and $HOMO_{-3}$ levels for CH_2XI (X=Br and I) in DFT calculations split further due to the spin-orbit interactions and generate more separated $HOMS_{-2}$ and $HOMS_{-3}$ in SO-DFT calculations. The closer the energy levels in DFT calculations, the larger the spin-orbit splitting in SO-DFT calculations. For CH_2I_2, the spin-orbit splitting between the HOMO and $HOMO_{-1}$ levels decrease the $HOMO_{-1}$ level and that of the $HOMO_{-2}$ and $HOMO_{-3}$ levels increase the $HOMO_{-2}$ level. Thus, the $HOMS_{-1}$ level is mainly from spin-orbit splitting of $HOMO_{-2}$ and the $HOMS_{-2}$ level is mainly from spin-orbit splitting of $HOMO_{-1}$ since the energy levels of HOMO, $HOMO_{-1}$, $HOMO_{-2}$, and $HOMO_{-3}$ are close as shown in Figure 1. The above interpretation of the spin-orbit splitting is an attempt to identify major factors. Since all molecular orbitals and also molecular spinors are mixtures of X and I atomic orbitals, additional orbital interactions play a role in determining accurate positions of energy levels.

Two stationary states, ^{2}A' and ^{2}A", of haloiodomethane cations were found from AREP calculations, and the geometries and vibrational frequencies of CH_2XI^+ molecules are summarized in Tables 6 and 7. The stable cation of haloiodomethane except CH_2ClI from AREP calculations is generated by the removal of an electron from the HOMO. The most stable cation of CH_2FI is the ^{2}A" state generated by the removal of an electron from the highest occupied a'' orbital. The most stable cation of CH_2XI (X=Br and I) is the ^{2}A' state generated by the removal of an electron from the highest occupied a' orbital while the most stable cation of CH_2ClI is the ^{2}A' state generated by the removal of an electron from the second highest occupied a' orbital. The ^{2}A' state has much smaller X-C-I angles than the neutral molecule in all CH_2XI, implying that the shape of the cation in this state is somewhat different from the neural molecule. On the contrary, the ^{2}A' state of the cation has the X-C-I angle similar to the neural molecule. Vibrational frequencies of the cation states do not differ too much for the X-C-I bending mode (ν_6 in Tables 5 and 7) except for CH_2FI. The two ^{2}A' and ^{2}A" states mix due to the spin-orbit interactions and generate two $^2E_{1/2}$ states. The energy differences of two cation states from AREP calculations for CH_2FI, CH_2ClI, CH_2BrI, and CH_2I_2 are 834, 1225, 2768, and 3584 cm^{-1} in Table 5. Energetically closer two states of cations of haloiodomethanes mix more substantially than energetically less close two states of cations. The geometries of CH_2XI^+ (X=F

Table 6. Geometries of CH_2XI (X = F, Cl, Br, and I) cation in the ground electronic state without (w/o) and with (w/) spin-orbit effects[a]

		bond length (Å)			bond angle (°)				Energy (in Hartree)
		C–X	C–I	C–H	X–C–I	X–C–H	I–C–H	H–C–H	
CH_2FI	$^2A'$	1.319	2.347	1.085	104.4	113.3	102.6	118.2	-174.6960
	$^2A''$	1.318	2.268	1.091	110.0	113.2	102.0	115.0	-174.6998
	$^2E_{1/2}$	1.318	2.300	1.088	108.1	113.3	102.0	116.4	-174.7132
CH_2ClI	$^2A'$	1.767	2.187	1.082	96.1	111.9	109.7	115.8	-165.4188
	$^2A''$	1.715	2.245	1.090	116.1	113.1	101.0	111.6	-165.4132
	$^2E_{1/2}$	1.738	2.242	1.084	106.0	112.7	104.9	114.5	-165.4309
CH_2BrI	$^2A'$	1.948	2.164	1.081	95.2	111.0	110.9	115.9	-306.4725
	$^2A''$	1.904	2.174	1.092	119.3	110.1	103.8	109.4	-306.4599
	calc.[b]	1.899	2.146	1.107	112.0	109.3	104.7	108.3	
	$^2E_{1/2}$	1.942	2.175	1.082	97.9	111.2	109.9	115.5	-306.4850
CH_2I_2	$^2A'$	2.161	2.161	1.082	96.3	110.9	110.9	115.3	-261.9331
	$^2A''$	2.144	2.144	1.091	122.0	106.4	106.4	108.5	-261.9168
	$^2E_{1/2}$	2.164	2.164	1.082	98.4	110.6	110.6	115.0	-261.9513

[a]The set **1** basis sets and RECPs in Table 1 were used. [b]B3LYP/Sadlej-PVTZ data from Ref.[46]

Table 7. Vibrational frequencies (in cm^{-1}) of CH_2XI (X = F, Cl, Br, and I) cation in the ground electronic state calculated without (w/o) and with (w/) spin-orbit effects[a]

		a′						*a″*		
		ν_1[b]	ν_2	ν_3	ν_4	ν_5	ν_6	ν_7	ν_8	ν_9
CH_2FI	$^2A'$	3097	1494	1261	1154	411	169	3221	1230	844
	$^2A''$	3041	1457	1257	1156	418	222	3127	1217	741
	$^2E_{1/2}$	3063	1471	1254	1150	404	206	3169	1223	795
CH_2ClI	$^2A'$	3126	1432	1167	719	499	160	3231	1066	828
	$^2A''$	3045	1385	1156	790	348	178	3096	1078	609
	$^2E_{1/2}$	3106	1420	1175	747	419	112	3206	1089	791
	exp.[c]		1385	1164	767	408	114		1072	
CH_2BrI	$^2A'$	3133	1413	1137	602	513	135	3243	1015	814
	$^2A''$	3034	1331	1084	642	430	147	3064	1017	477
	$^2E_{1/2}$	3126	1410	1136	601	505	116	3233	1022	800
	exp.[d]			1208	619	482	116			
CH_2I_2	$^2A'$	3130	1401	1082	545	506	116	3235	979	770
	$^2A''$	3044	1321	1053	590	448	124	3068	983	384
	$^2E_{1/2}$	3127	1395	1075	530	507	103	3230	982	753

[a]The set **1** basis sets and RECPs in Table 1 were used. [b]Mulliken notation. [c]MATI spectroscopic data from Ref.[11,12] [d]MATI spectroscopic data from Ref.[13]

and Cl) from SO-DFT calculations are roughly in the middle of two cation geometries from DFT calculations since two cation states of CH_2XI (X=F and Cl) from DFT calculations are energetically close enough to mix two cation states. In contrast, the geometries of CH_2XI (X=Br and I) from SO-DFT calculations are close to those of more stable cations from DFT calculations since two cation states of CH_2XI (X=Br and I) from DFT calculations are energetically not so close enough to produce well mixed fine-structure states. In this sense, large spin-orbit induced shape change is predicted for CH_2FI and CH_2ClI, but not for CH_2BrI and CH_2I_2. One confirmation of this is the X-C-I bending mode in Table 7 since this ν_6 bending mode reflects bonding property of the X-C-I bond angle. Energetics of spin-orbit effects will be important in analyzing PES data, but this is not attempted here.

Conclusion

The importance of including spin-orbit interactions for the correct description of structures and vibrational frequencies of haloiodomethanes is demonstrated by DFT calculations with spin-orbit relativistic effective core potentials. The vibrational frequencies and the molecular geometries obtained by SO-DFT calculations do not match with the experimental results as well as for other cations without significant relativistic effects. In this sense, the present data can be considered as a guideline in the development of the relativistic quantum chemical methods. The influence of spin-orbit effects on the bending frequency of the cation could be recognized by comparing the experimental and calculated results.

Spin-orbit effects on the geometries and vibrational frequencies of CH_2XI (X=F, Cl, Br, and I) neutral are negligible except that C-I bond lengths of haloiodomethane neutral is slightly increased by the inclusion of spin-orbit effects. The $^2A'$ and $^2A''$ states were found in the cations of haloiodomethanes and mix due to the spin-orbit interactions and generate two $^2E_{1/2}$ fine-structure states. The energy differences of two cation states from AREP calculations for CH_2FI^+, CH_2ClI^+, CH_2BrI^+, and $CH_2I_2^+$ are 834, 1225, 2768, and 3584 cm^{-1}. The geometries of CH_2XI^+ (X=F and Cl) from SO-DFT calculations are roughly in the middle of two cation geometries from DFT calculations since two cation states of CH_2XI (X=F and Cl) from DFT calculations are energetically close enough to mix two cation states. The geometries of CH_2XI^+ (X=Br and I) from SO-DFT calculations are close to that of most stable cation from DFT calculations since two cation states of CH_2XI (X=Br and I) from DFT calculations are energetically not close enough near the fine-structure state minimum to extensively mix two cation states.

Acknowledgments. This paper is dedicated to Professor Myung Soo Kim on the occasion of his honourable retirement. Authors also thank Professor Myung Soo Kim and Dr. M. Kim for the collaboration in the study of chloro- and bromo- iodomethanes, which initiated this work. The research is supported by grants (2007-0056095, 2012-R1A1A2000915) from National Research Foundation funded by Korea government. Computational resouces were partly provided by KISTI (KSC-2012-C2-81).

References

1. Christiansen, P. A.; Ermler, W. C.; Pitzer, K. S. *Annu. Rev. Phys. Chem.* **1985**, *36*, 407.
2. Pyykkö, P. *Adv. Quantum Chem.* **1978**, *11*, 353.
3. Lee, Y. S.; McLean, A. D. *J. Chem. Phys.* **1982**, *76*, 735.
4. Lee, Y. S. In *Relativistic Electronic Structure Theory, Part 2: Applications*; Schwerdtfeger, P., Ed.; Elsevier, B. V.: Amsterdam, The Netherlands, 2004; Vol. 14.
5. Lee, H. S.; Cho, W. K.; Choi, Y. J.; Lee, Y. S. *Chem. Phys.* **2005**,

311, 121.
6. Fossgaard, O.; Gropen, O.; Valero, M. C.; Saue, T. *J. Chem. Phys.* **2003**, *118*, 10418.
7. Han, Y.-K.; Bae, C.; Son, S.-K.; Lee, Y. S. *J. Chem. Phys.* **2000**, *112*, 2684.
8. Choi, Y. J.; Lee, Y. S. *J. Chem. Phys*. **2003**, *119*, 2014.
9. Kendall, R. A.; Apra, E.; Bernholdt, D. E.; Bylaska, E. J.; Dupuis, M.; Fann, G. I.; Harrison, R. J.; Ju, J.; Nichols, J. A.; Nieplocha, J.; Straatsma, T. P.; Windus, T. L.; Wong, A. T. *Computer Phys. Comm.* **2000**, *128*, 260.
10. Straatsma, T. P.; Apra, E.; Windus, T. L.; Dupuis, M.; Bylaska, E. J.; Jong, W. d.; Hirata, S.; Smith, D. M. A.; Hackler, M. T.; Pollack, L.; Harrison, R. J.; Nieplocha, J.; Tipparaju, V.; Krishnan, M.; Brown, E.; Cisneros, G.; Fann, G. I.; Früchtl, H.; Garza, J.; Hirao, K.; Kendall, R.; Nichols, J. A.; Tsemekhman, K.; Valiev, M.; Wolinski, K.; Anchell, J.; Bernholdt, D.; Borowski, P.; Clark, T.; Clerc, D.; Dachsel, H.; Deegan, M.; Dyall, K.; Elwood, D.; Glendening, E.; Gutowski, M.; Hess, A.; Jaffe, J.; Johnson, B.; Ju, J.; Kobayashi, R.; Kutteh, R.; Lin, Z.; Littlefield, R.; Long, X.; Meng, B.; Nakajima, T.; Niu, S.; Rosing, M.; Sandrone, G.; Stave, M.; Taylor, H.; Thomas, G.; Lenthe, J. V.; Wong, A.; Zhang, Z. Pacific Northwest National Laboratory: Richland, Washington 99352-0999, USA, 2003.
11. Lee, M.; Kim, H.; Lee, Y. S.; Kim, M. S. *Angew. Chem. Int. Ed.* **2005**, *44*, 2929.
12. Lee, M.; Kim, H.; Lee, Y. S.; Kim, M. S. *J. Chem. Phys.* **2005**, *122*, 244319.
13. Lee, M.; Kim, H.; Lee, Y. S.; Kim, M. S. *J. Chem. Phys.* **2005**, *123*, 024310.
14. Bilde, M.; Wallington, T. J.; Ferronato, C.; Orlando, J. J.; Tyndall, G. S.; Estupiñan, E.; Haberkorn, S. *J. Phys. Chem. A* **1998**, *102*, 1976.
15. Vogt, R.; Sander, R.; Glasow, R. V.; Crutzen, P. J. *J. Atmos. Chem.* **1999**, *32*, 375.
16. Finalayson-Pitts, B. J.; Pitts Jr., J. N. *Chemistry of the Upper and Lower Atmosphere*; Academic: San Diego, 2000.
17. Alicke, B.; Hebestreit, K.; Stutz, J.; Platt, U. *Nature* **1999**, *397*, 572.
18. Solomon, S.; Garcia, R. R.; Ravishankara, A. R. *J. Geophys. Res.* **1994**, *99*, 20491.
19. Man, S.-Q.; Kwok, W. M.; Johnson, A. E.; Phillips, D. L. *J. Chem. Phys.* **1996**, *105*, 5842.
20. Arashkevich, D. G.; Sharpiro, M.; Brumer, P. J. *Chem. Phys.* **2002**, *116*, 5584.
21. Liu, K.; Zhao, H.; Wang, C.; Zhang, A.; Ma, S.; Li, Z. *J. Chem. Phys.* **2005**, *122*, 044310.
22. Eland, J. H. *Photoelectron Spectroscopy*; Butterworth: Southhampton, 1984.
23. Novak, I.; Benson, J. M.; Potts, A. W. *Chem. Phys.* **1986**, *107*, 129.
24. Ford, M. S.; Tong, X.; Dessent, C. E. H.; Müller-Dethlefs, K. *J. Chem. Phys.* **2003**, *119*, 12914.
25. Seiler, R.; Hollenstein, U.; Softley, T. P.; Merkt, F. *J. Chem. Phys.* **2003**, *118*, 10024.
26. Georgiev, S.; Neusser, H. J.; Chakraborty, T. *J. Chem. Phys.* **2004**, *120*, 8015.
27. Lee, Y. S.; Ermler, W. C.; Pitzer, K. S. *J. Chem. Phys.* **1977**, *67*, 5861.
28. Ermler, W. C.; Lee, Y. S.; Christiansen, P. A.; Pitzer, K. S. *Chem. Phys. Lett.* **1981**, *81*, 70.
29. Stephens, P. J.; Devlin, F. J.; Chabalowski, C. F.; Frisch, M. J. *J. Phys. Chem.* **1994**, *98*, 11623.
30. Becke, A. D. *J. Chem. Phys.* **1993**, *98*, 5648.
31. Lee, C.; Yang, W.; Parr, R. G. *Phys. Rev. B* **1988**, *37*, 785.
32. Hurley, M. M.; Pacios, L. F.; Christiansen, P. A.; Ross, R. B.; Ermler, W. C. *J. Chem. Phys.* **1986**, *84*, 6840.
33. LaJohn, L. A.; Christiansen, P. A.; Ross, R. B.; Atashroo, T.; Ermler, W. C. *J. Chem. Phys.* **1987**, *87*, 2812.
34. Adamo, C.; Barone, V. *J. Chem. Phys.* **1998**, *110*, 6158.
35. Ernzerhof, M.; Scuseria, G. E. *J. Chem. Phys.* **1999**, *110*, 5029.
36. Slater, J. C. *Quantum Theory for Molecular and Solids*. Vol. 4: *The Self-Consistent Field for Molecular and Solids*; McGraw-Hill: New York, 1974.
37. Vosko, S. H.; Wilk, L.; Nusair, M. *Can. J. Phys.* **1980**, *58*, 1200.
38. Becke, A. D. *J. Chem. Phys.* **1988**, *88*, 3098.
39. Perdew, J. P. *Phys. Rev. B* **1986**, *33*, 8822.
40. Zhao, Y.; Truhlar, D. G. *J. Phys. Chem. A* **2004**, *108*, 6908.
41. Kim, J.; Ihee, H.; Lee, Y. S. *Theor. Chem. Acc.* **2011**, *129*, 343.
42. Ohkoshi, I.; Niide, Y.; Takano, M. *J. Mol. Spectrosc.* **1987**, *124*, 118.
43. Kudchadker, S. A.; Kudchadker, A. P. *J. Phys. Chem. Ref. Data* **1975**, *4*, 457.
44. Liu, Y.-J.; Ajitha, D.; Krogh, J. W.; Alexander, K.; Tarnovsky, N.; Lindh, R. *Chemphyschem* **2006**, *7*, 955.
45. Liu, Y. J.; De Vico, L.; Lindh, R.; Fang, W. H. *Chemphyschem.* **2007**, *8*, 890.
46. Zheng, X.; Phillips, D. L. *J. Chem. Phys.* **2000**, *113*, 3194.
47. Odelius, M.; Dai, M.; Davidsson, J.; Tarnovsky, A. N. *J. Chem. Phys.* **2004**, *121*, 2208.
48. Glukhovtsec, M. N.; Bach, R. D. *Chem. Phys. Lett.* **1997**, *269*, 145.
49. Marshall, P.; Srinivas, G. N.; Schwartz, M. *J. Phys. Chem. A* **2005**, *109*, 6371.
50. Duschek, F.; Schmitt, M.; Vogt, P.; Materny, A.; Kiefer, W. *J. Raman. Spectrosc.* **1997**, *28*, 445.
51. Sablinskas, V.; Klaeboe, P.; Nielsen, C. J.; Sülzle, D. *Analyst* **1992**, *117*, 365.
52. Kwok, W. M.; Phillips, D. L. *Chem. Phys. Lett.* **1995**, *235*, 260.